Heat Aging Effects on the Material Property and the Fatigue Life of Vulcanized Natural Rubber, and Fatigue Life Prediction Equations

Jae-Hyeok Choi, Hee-Jin Kang, Hyun-Yong Jeong*, Tae-Soo Lee
Department of Mechanical Engineering, Sogang University,
1 Shinsoo-Dong, Mapo-Gu, Seoul 121-742, Korea
Sung-Jin Yoon
Research and Development Division, Hyundai Motor Company,
772-1 ChangDuk-Dong HwaSeong-Si Kyonggi-Do 445-707, Korea

When natural rubber is used for a long period of time, it becomes aged ; it usually becomes hardened and loses its damping capability. This aging process affects not only the material property but also the (fatigue) life of natural rubber. In this paper the aging effects on the material property and the fatigue life were experimentally investigated. In addition, several fatigue life prediction equations for natural rubber were proposed. In order to investigate the aging effects on the material property, the load-stretch ratio curves were plotted from the results of the tensile test, the compression test and the simple shear test for virgin and heat-aged rubber specimens. Rubber specimens were heat-aged in an oven at a temperature ranging from 50℃ to 90℃ for a period ranging from 2 days to 16 days. In order to investigate the aging effects on the fatigue life, fatigue tests were conducted for differently heat-aged hourglass-shaped and simple shear specimens. Moreover, finite element simulations were conducted for the specimens to calculate physical quantities occurring in the specimens such as the maximum value of the effective stress, the strain energy density, the first invariant of the Cauchy-Green deformation tensor and the maximum principal nominal strain. Then, four fatigue life prediction equations based on one of the physical quantities could be obtained by fitting the equations to the test data. Finally, the fatigue life of a rubber bush used in an automobile was predicted by using the prediction equations, and it was compared with the test data of the bush to evaluate the reliability of those equations.

Key Words : Heat-aging Effect, Natural Rubber, Fatigue Life, Fatigue Life Prediction Equation

1. Introduction

Natural rubber has characteristics of large elastic deformation with hysteretic loss and incompressibility. In addition, it can be readily manufactured at a comparatively low cost. Because of these characteristics, rubber is widely used in numerous products such as automobiles, locomotives and commodities (Treloar, 1975). However, it is difficult to develop a design methodology for rubber components because the material property of rubber changes drastically depending on raw materials (composition), manufacturing conditions (mixing and curing conditions), loading conditions (strain, strain rate, temperature) and

* Corresponding Author,
E-mail : jeonghy@sogang.ac.kr
TEL : +82-2-705-8640; **FAX** : +82-2-712-0799
Department of Mechanical Engineering, Sogang University, 1 Shinsoo-Dong, Mapo-Gu, Seoul 121-742, Korea. (Manuscript **Received** April 19, 2004; **Revised** April 6, 2005)

even the period of usage. When rubber is used for a long period of time, rubber becomes aged ; it usually becomes hardened and loses its damping capability. This aging process results mainly from heat due to hysteretic loss, and it affects not only the material property but also the (fatigue) life of rubber.

In this paper the heat-aging effects on the material property and the fatigue life of natural rubber were experimentally investigated. In addition, several fatigue life prediction equations were proposed based on the fatigue test data and FEM (Finite Element Method) simulation results. In order to determine the material property, the load-stretch ratio curves were plotted from the results of the tensile test, the compression test, and the simple shear test for virgin and heat-aged rubber specimens. The aged specimens were heat-aged in an oven set at a temperature ranging from 50℃ to 90℃ for a period ranging from 2 days to 16 days. When a specimen was aged in an oven, a cylinder-shaped compression test specimen was aged together. The hardness of the compression test specimen was measured by using Durometer type A (ASTM D2240), and it was assumed to be the same as the hardness of the specimen. The hardness was also regarded as an indicator of the aging amount. The crosslink density would be a better indicator, but it is more convenient to measure the hardness not only of the specimens but also of rubber components.

Fatigue tests were conducted for hourglass-shaped specimens and for simple shear specimens. All the specimens were aged in different amounts, and the hardness of the specimens was measured. In this way, the fatigue life of the aged specimens could be represented as a function of hardness. In addition, FE simulations were conducted on the specimens to obtain the maximum value of the effective stress, the strain energy density, the first invariant of the Cauchy-Green deformation tensor and the maximum principal nominal strain occurring in the specimens. Then, four fatigue life prediction equations based on one of those four physical quantities could be obtained by fitting the equations to the test data. Finally, a rubber bush used in an automobile was aged, and fatigue test was conducted for the bush. An FE simulation for the rubber bush was conducted, and the maximum values of those four physical quantities were obtained. By plugging the maximum values into the fatigue life prediction equations, the fatigue life of the rubber bush was predicted. This predicted fatigue life was compared with the fatigue test data. All of the four prediction equations resulted in a reasonably good correlation with the test data, and among the prediction equations, the strain energy density equation resulted in a slightly better correlation. Therefore, it may be concluded that the strain energy density is a feasible controlling physical quantity in the fatigue failure of natural rubber.

2. Material Tests

2.1 Tensile test

The material responses of rubber depend on the composition, additives, and mixing and curing processes. In this study, the rubber actually used in the rubber bushes of an automobile was chosen as the test material. The dumbbell-shaped test specimen with gage length of 20 mm and thickness of 3 mm was used at the tensile test (ASTM D412). The specimen was punched out from a sheet, and was left at room temperature (23℃) for at least 3 hours before testing. The specimen was loaded by a UTM at a speed of 500 mm/min, and the deflection was measured by using an extensometer (Findik, 2004).

The deflection can be represented by a stretch ratio, which is the ratio of the deformed length to the undeformed length. The load-stretch ratio curve of a vulcanized natural rubber changes during first several repeated loadings, and this is called the Mullins effect (Mullin, 1969). This effect is due to gradual orientation of molecular chains. Thus, the load-stretch ratio curve obtained at the first loading is not representative of the material property, and mechanical conditioning should be conducted before obtaining a representative load-stretch ratio curve (Brown, 1986). As shown in Fig. 1, there is a noticeable difference between the load-stretch ratio curves obtained at the first and the second loadings. How-

ever, there is a negligible difference after the third loading, and it has been decided to regard the load-stretch ratio curve obtained at the fourth loading as the representative load-stretch ratio curve. In order for the specimen to recover from the previous loading, the specimen was left unloaded for 10 min before the next loading (Shen, 2001).

In Fig. 2, two load-stretch ratio curves obtained from different mechanical conditioning are shown. One is the curve obtained from mechanical conditioning up to the stretch ratio $\lambda=1.7$, and the other is the curve obtained from mechanical conditioning up to the stretch ratio $\lambda=3.0$. Since the curve of a more mechanically conditioned specimen is lower than the other one due to strain softening, it is important to specify the maximum stretch ratio when the load-stretch ratio curve of a vulcanized natural rubber is obtained or shown. In this study, it was decided to conduct mechanical conditioning with the stretch ratio of 1.7 because the automobile rubber bush under investigation seemed to have a stretch ratio of 1.7 according to an FE simulation.

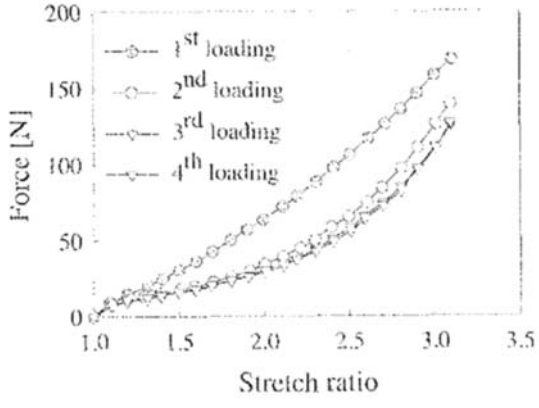

Fig. 1 Mullins effects on the tensile load-stretch ratio curve of natural vulcanized rubber

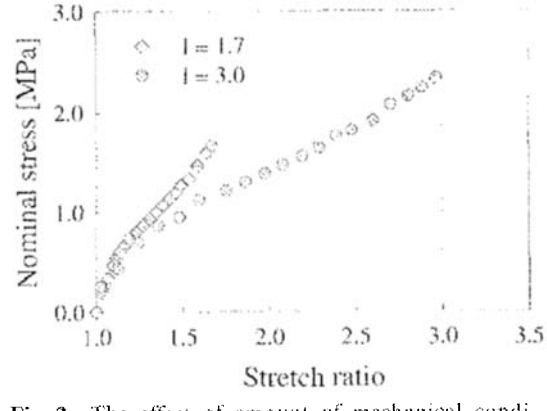

Fig. 2 The effect of amount of mechanical conditioning on the tensile load-stretch ratio curve

2.2 Compression test

A cylinder-shaped specimen with diameter of 28.8 mm and height of 12.5 mm was used at the compression test, and the compression test was conducted by a UTM at a speed of 12.5 mm/min according to ASTM (ASTM 575). Since the effect of mechanical conditioning on the compression specimen was comparatively small, a representative load-stretch ratio curve was obtained at the third loading being almost the same as the load-stretch ratio curve obtained at the second loading. It is well known that barreling occurs at a compression test due to friction between a specimen and a loading plate. In order to prevent barreling, a lubricant was applied on the top and bottom surfaces of the specimen.

2.3 Shear test

Shear tests were conducted on two different specimens ; simple shear specimen and pure shear specimen. As shown in Fig. 3, the simple shear specimen was designed to be in a dimension of $25\times12.5\times12.5$ mm and to have fillets rounded by 3 mm to prevent stress concentration (Lee, 1988). The rubber was injected against the end plates, and it was cooled down with the end plates at-

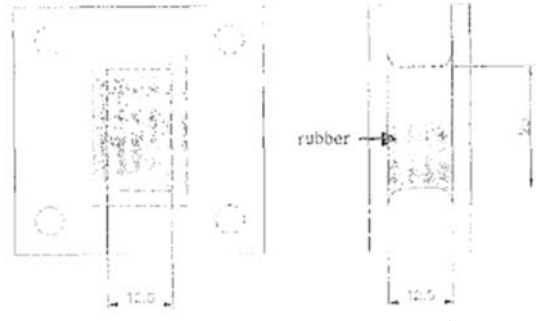

Fig. 3 A simple shear specimen with fillets

tached. This resulted in uniform attachment over the contact area. The simple shear test was conducted on a UTM at a speed of 25 mm/min according to ISO (1827), and a load-stretch ratio curve was obtained at the fourth loading as at the tensile test.

As shown in Fig. 4, a pure shear specimen was designed to have a rubber sheet glued between two transparent plastic plates, and its dimension was 100×10×2 mm (Shin, 1998). The width was designed to be 10 times the height in order to have pure shear deformation. The pure shear specimen was pulled by a UTM at the same speed as at the simple shear test, and a load-stretch ratio curve was obtained from the fourth loading. Of course, the pure shear test was regarded successful only when the rubber sheet was not detached from the plastic plates, which could be examined by naked eyes. Two load-stretch ratio curves are shown in Fig. 5; one was obtained at the simple shear test, and the other was obtained at the pure shear test. Note that there is almost no difference at low stretch ratios, but there is a noticeable difference at high stretch ratios.

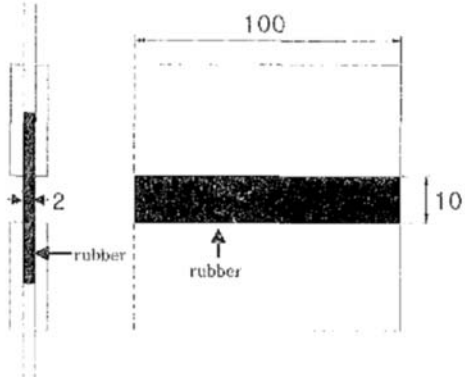

Fig. 4 A pure shear specimen with rubber glued between two transparent plates

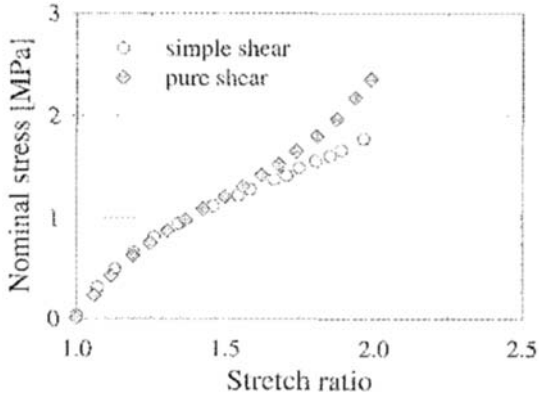

Fig. 5 Comparison of simple shear test curve with pure shear test curve

3. Material Property Change Due to Heat Aging

3.1 High and low temperature aging

Rubber becomes hardened as it experiences cyclic loading. During cycling loading, its temperature increases due to heat converted from hysteretic loss, and this causes aging (Brown, 1986). The aging process leads not only to mechanical property change but also to chemical structure change so called degradation. Among mechanical property changes, a hardness change can be easily detected, and it can be converted to the elastic modulus change (ASTM D1415). However, it requires considerable amount of time to investigate the aging effects at a nominal condition. In order to speed up the aging process and to measure a hardness change in a reasonable time, a rubber specimen can be heat-aged in an oven set at a certain temperature for a certain period of time.

Rubber usually becomes more hardened when it is heated at a higher temperature or for a longer time. However, when the rubber was heat-aged at a temperature over 90℃ even for a period of 48 hours, it became so much hardened that some cracks occurred on the surface. The heat aging in this study was a process to accelerate the aging process in normal operating conditions, which hardly causes surface cracking. Thus, three tensile specimens were heat-aged at 90℃ for 48 hours, 96 hours, and 192 hours, respectively, and they were left in the room temperature for a day before being tested. In Fig.6, the load-stretch ratio curves obtained from the tensile test are shown for a virgin specimen and the three aged specimens. Note that the rubber became more hardened as the heat-aging period increased, and especially

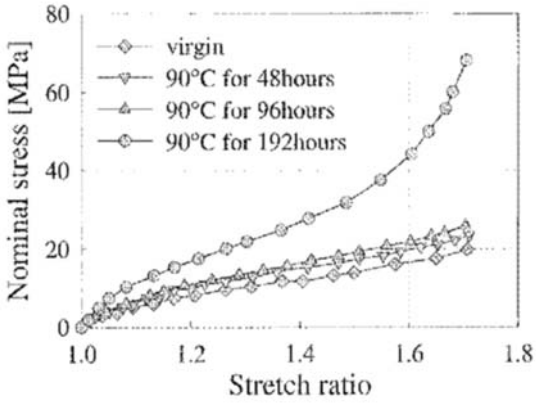

Fig. 6 Load-stretch ratio curves obtained from the tensile test for four differently aged specimens

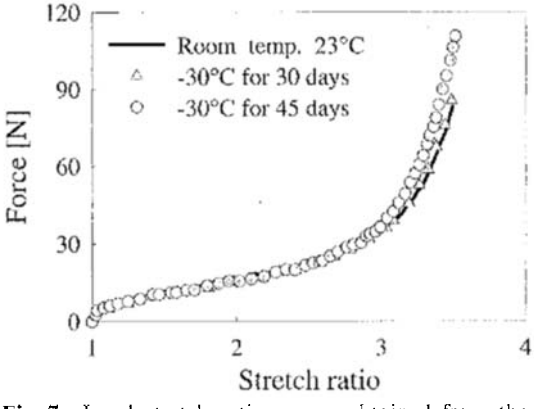

Fig. 7 Load-stretch ratio curves obtained from the tensile test for virgin rubber and once-frozen rubber

the rubber specimen heat-aged for 192 hours became hardened significantly.

In contrast, rubber does not show any noticeable material property change after a long period of freezing. Specimens were kept frozen at −30℃ for 15 days, 30 days, and 45 days, respectively, and they were left in room temperature for a day before being tested. In Fig. 7, the load-stretch ratio curves obtained from the tensile test are shown, and they show no major difference between the once-frozen specimens and the virgin specimen.

3.2 High and low temperature environment tests

In this study, rubber specimens were also tested

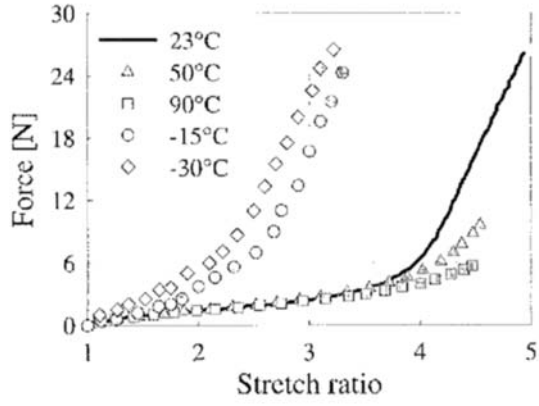

Fig. 8 Load-stretch ratio curves obtained from the tensile test conducted in a temperature-controlled chamber

in a temperature-controlled chamber. Before being tested, a specimen was kept in a chamber for 10 min to help it reach a uniform temperature. Note that the trend of load-stretch ratio curve change in this environment test was almost opposite to that observed in the aging test. Figure 8 shows the load-stretch ratio curves obtained from the tensile test, and rubber shows a stiffer response at a low temperature than at room temperature. The curve becomes higher as the temperature drops from room temperature to −15℃, and to −30℃. However, rubber does not show any noticeable difference at a high temperature below the stretch ratio of 2.5 although it shows slightly softer response over the stretch ratio of 2.5.

3.3 Hardness change due to heat aging

In this study the compression specimen was heat-aged in an oven, and its hardness in IRHD was measured by using Durometer type A according to ASTM (ASTM D2240). The specimen was heat-aged at a temperature between 50℃ and 90℃ for a period of between 48 hours and 384 hours. The test data of hardness change for the specimens heat-aged at different temperatures are shown as symbols in Fig. 9 as a function of period. The hardness increases as the heat-aging temperature and/or the heat-aging period increase.

A material property change of a polymer due to

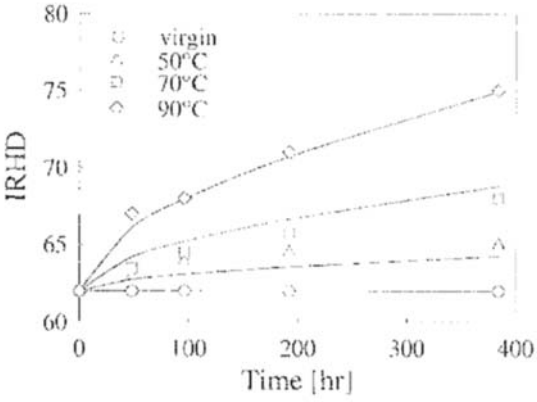

Fig. 9 Hardness of rubbers aged at different temperatures as a function of aging period

temperature is usually represented by Arrhenius equation in which the logarithmic value of a material property is assumed to be inversely proportional to temperature (Miller, 1966). However, the hardness increases as the heat-aging temperature increases, and the hardness change is a function of the heat-aging period as well as the temperature. Thus, a hardness prediction equation was proposed as follows, the effects both of the temperature and of the period being taken into account.

$$K_1 = LOG(T/23)^{2.958} \quad (1)$$

$$K_2 = (t/477.2)^{0.5263} \quad (2)$$

$$IRHD = 62 * EXP[K_1 * K_2] \quad (3)$$

Here, K_1 and K_2 are the parameters that account for the effect of temperature and the period, respectively, and T is the heat-aging temperature in ℃, and t is the heat-aging period in hour. The constant 62 in Eq. (3) is the hardness of the virgin rubber with no aging, and the exponents in Eqs. (1) and (2) were determined by using the least square method. The hardness predicted by Eq. (3) is shown as curves in Fig. 9 along with the test data. Note that the curves do not perfectly fit to the test data but they follow the trend of the data.

Next, the hardness change of specimens heat-aged subsequently at two different conditions was investigated. Several specimens were heat-aged at 50℃ or 70℃ for 384 hours first, and then they were heat-aged at 90℃ for four different periods. In order to predict the hardness change in this case, Eq. (3) had to be modified slightly as follows.

$$IRHD = (62 + K_1 + K_2) * EXP[K_1' * K_2'] \quad (4)$$

Here, K_1 and K_2 account for the damage due to the first heat aging process, and K_1' and K_2' account for the damage due to the second heat aging process. Of course, the parameters could be easily calculated from Eqs. (1) and (2), and the damage due to the first heat aging process was taken into account as the increased initial hardness in Eq. (4). In Table 1 and Table 2, the test data on the hardness of specimens heat-aged twice are compared with the predicted hardness from Eq. (4). Note that the predicted hardness values are in a good agreement with test data.

Table 1 Comparison of predicted hardness with measured hardness for specimens heat-aged initially at 50℃

Initial condition	Final condition	Measured IRHD	Predicted IRHD	Error (%)
Heat age at 50℃ for 384 hours	90℃ 48hr	67.22	67.06	0.23
	90℃ 96hr	68.53	68.96	0.63
	90℃ 192hr	71.51	71.79	0.39
	90℃ 384hr	35.69	76.07	0.50

Table 2 Comparison of predicted hardness with measured hardness for specimens heat-aged initially at 70℃

Initial condition	Final condition	Measured IRHD	Predicted IRHD	Error (%)
Heat age at 50℃ for 384 hours	90℃ 48hr	68.42	67.14	1.87
	90℃ 96hr	69.02	69.04	0.03
	90℃ 192hr	71.33	71.88	0.99
	90℃ 384hr	75.92	76.17	0.32

4. Coefficients of Strain Energy Potentials

4.1 Load-stretch ratio curves of heat-aged specimens

As mentioned previously, the hardness change has a trend; it increases monotonically as the

temperature and/or the period of the heat-aging process increase. This implies that the hardness can be an indicator for the material behavior change due to heat-aging. In order to investigate the feasibility of using the hardness as an indicator for the material behavior of heat-aged rubber, the tensile test and the compression test were conducted for specimens heat-aged at several conditions ; they were heat-aged at 50℃, 70℃ or 90℃ for 48, 96, 192 or 384 hours. The load-stretch ratio curves are shown in Fig. 10 for specimens with different IRHD's, and it is obvious that the rubber becomes stiffer over the wide range of the extension ratio as the IRHD increases. In addition, the load-stretch ratio curves of two specimens heat-aged differently but in similar IRHD's are shown in Fig. 11. Note that the load-stretch ratio curve for IRHD=64.3 is slightly higher but similar to that for IRHD=64.0. Therefore, the hardness can be regarded as an indicator for the material behavior of heat-aged rubber specimens.

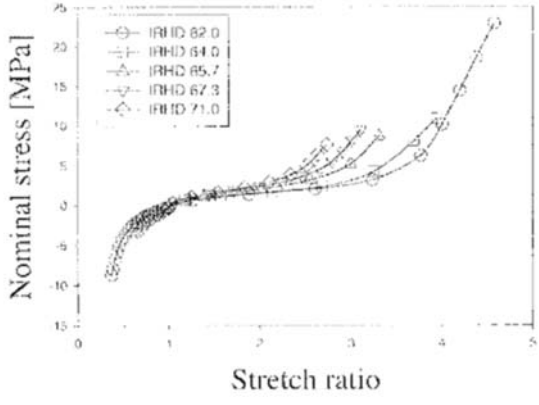

Fig. 10 Load stretch ratio curves for rubber specimens heat-aged in different amounts

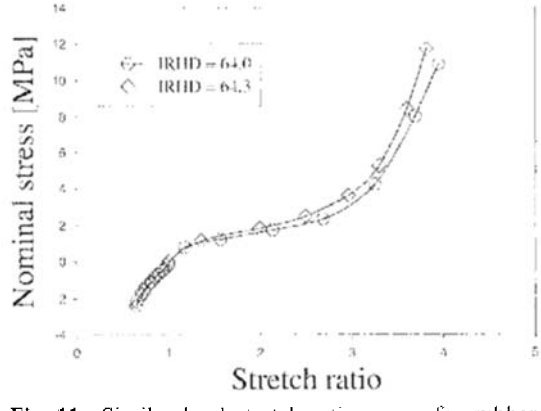

Fig. 11 Similar load-stretch ratio curves for rubber specimens with similar IRHD's

4.2 Coefficients in Mooney-Rivlin model

Rubber is usually assumed to be a hyperelastic material, and its strain energy can be represented by a function of invariants of the Cauchy-Green deformation tensor or the principal stretches. Among several strain energy functions, Mooney-Rivlin model given in Eq. (5) and Ogden model given in Eq. (6) are widely used (Rivlin, 1956 ; Ogden, 1986).

$$W=A_{10}(I_1-3)+A_{01}(I_2-3) \tag{5}$$

$$W=\sum_{i=1}^{3}\frac{2\mu_i}{\alpha_i^2}(\lambda_1^{\alpha_i}+\lambda_2^{\alpha_i}+\lambda_3^{\alpha_i}-3) \tag{6}$$

Here, A_{10}, A_{01}, μ_i, and α_i are material coefficients.

The Ogden model is better to fit the test data over a stretch ratio of 2.5 than the Mooney-Rivlin model. However, the coefficients in the Ogden model are not unique (i.e. there exist several sets of coefficients that fit a load-stretch ratio curve), and they do not have similar values even for similar load-stretch ratio curves. Thus, in this study the Mooney-Rivlin model was decided to be used mainly because in the rubber bush under investigation the stretch ratio hardly reaches 2.5 and the coefficients in the Mooney-Rivelin model are unique.

In order to investigate the change of the coefficients in the Mooney-Rivlin model caused by heat-aging, the tensile and compression tests were conducted for virgin and heat-aged rubbers, and A_{10} and A_{01} were obtained by using the least square method available in ABAQUS, a commercial FEM code (ABAQUS, 2001). In Fig. 12, A_{10} and A_{01} are plotted as a function of IRHD. Note that A_{10} and A_{01} remain almost constant at 0.760 and −0.067, respectively, until IRHD reaches about 69, but they change significantly over IRHD of about 69 and reach 1.707 and −0.557, respectively. This implies that the material behavior of the rubber changes significantly around IRHD of 69.

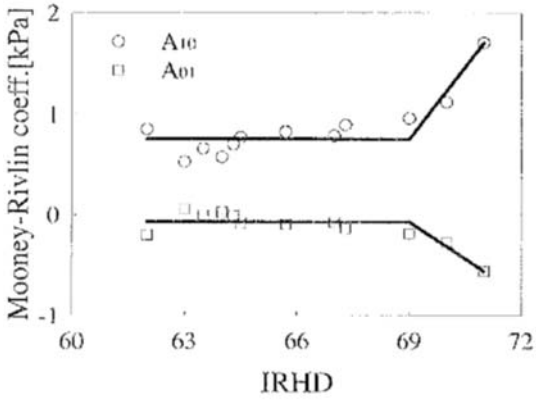

Fig. 12 Mooney-Rivlin coefficients A_{10} and A_{01} for differently heat-aged specimens shown as a function of IRHD

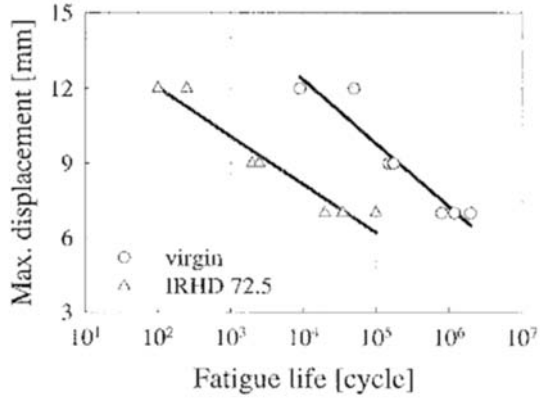

Fig. 13 Fatigue life of virgin and heat-aged simple shear specimens as a function of the maximum displacement

5. Fatigue Test

5.1 Fatigue test on specimens

Fatigue tests were conducted by using MTS 810, and the tests were displacement-controlled at a rate of 3 Hz with the minimum displacement of 0 mm and the maximum displacement of 7, 9 or 12 mm (Takeuchi, 1993). During the tests, the specimen was cooled by compressed air, and the temperature around it was kept at 23±2℃.

First, the fatigue test was conducted for the simple shear specimen shown in Fig. 3, and the fatigue life was determined to be the number of cycles at which a crack at a size of about 3 mm could be seen by naked eyes. This way of determining a fatigue life is often conducted in industry because the load does not drop noticeably even with a crack of about 3 mm long, and the fatigue life may be overestimated if it is determined based on the load drop. In Fig. 13, the fatigue lives of virgin rubber specimens and heat-aged specimens with IRHD of 72.5 are shown as a function of the maximum displacement. As expected, the fatigue life decreases as the maximum displacement increases. In addition, the decreasing rate of the fatigue life seems to be similar for the virgin and heat-aged specimens.

Next, the fatigue test was conducted for an hourglass-shaped specimen designed by Takeuchi et al.(1993). As shown in Fig. 14, the hourglass-shaped specimen has an oval-shaped cross section

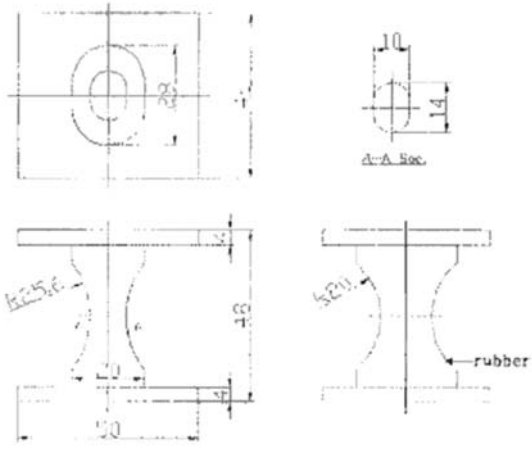

Fig. 14 Hourglass-shaped fatigue test specimen design by Takeuchi et al.(1993)

at the center, and the seam line is located at the surface of the minor axis. Thus, during the test the maximum tensile or compressive stress occurs at the surface of the major axis, where a crack usually occurs. Unlike the case of the simple shear specimen, the fatigue life was determined to be the number of cycles at which the maximum vertical load became half of the vertical load at 10,000 cycles because a crack grew comparatively fast once it was created and the load dropped accordingly unlike the case of the simple shear specimen (Takeuchi, 1993). As shown in Fig. 15, the fatigue life decreases as the maximum displacement increases, and the decreasing rate seems to be

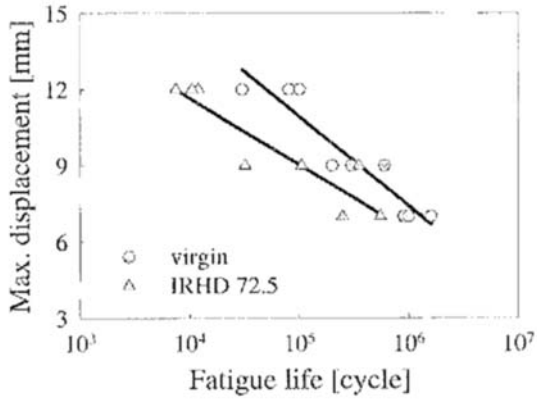

Fig. 15 Fatigue life of virgin and heat-aged hourglass-shaped specimens as a function of maximum displacement

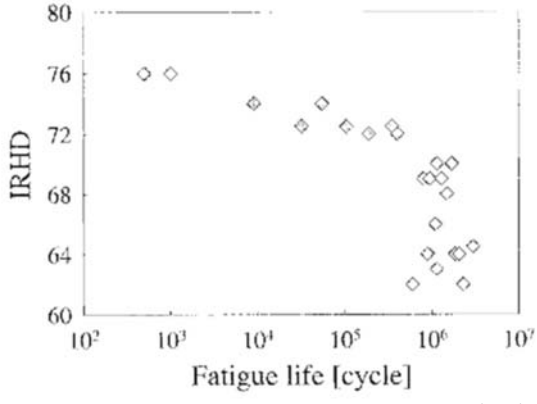

Fig. 16 Fatigue life of virgin and heat-aged simple shear specimens at a maximum displacement of 9 mm shown as a function of IRHD

similar for the virgin and heat-aged specimens. However, the difference of fatigue life between the virgin rubber and the heat-aged rubber is not as large as that at the simple shear fatigue test.

In order to investigate the effect of heat-aging on the fatigue life, the fatigue test was conducted for many differently heat-aged specimens at the maximum displacement of 9 mm, which was the median of the maximum displacements chosen previously. The fatigue life is shown as a function of IRHD in Fig. 16 for the simple shear specimen and in Fig. 17 for the hourglass-shaped specimen. Note that in both specimens the fatigue life seems to remain almost the same below

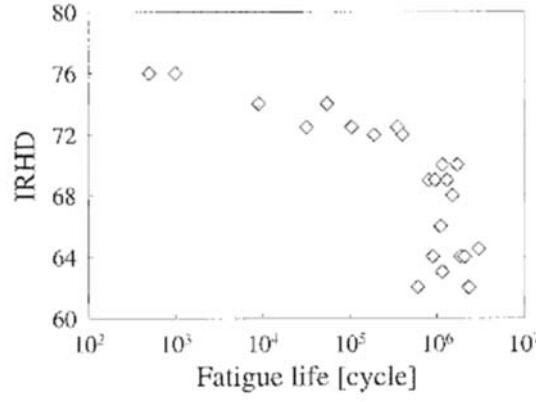

Fig. 17 Fatigue life of virgin and heat-aged hourglass-shaped specimens at a maximum displacement of 9 mm shown as a function of IRHD

IRHD of about 70, but it decreases sharply over IRHD of about 70.

5.2 Fatigue test on an automobile bush

Fatigue tests were conducted for a rubber bush used in a lower control arm by using Instron 8500 plus, and they were conducted under a sinusoidal load from 0 to 600 kgf at a rate of 3 Hz. In order to investigate the effect of aging, the bush was also heat-aged in different conditions, and it was fatigue-tested. In addition, the tests were conducted along two different loading directions as shown in Fig. 18, and the bush was air-cooled throughout the test. As in the case of the simple shear specimen, the fatigue life of the bush was determined to be the number of cycles at which a crack

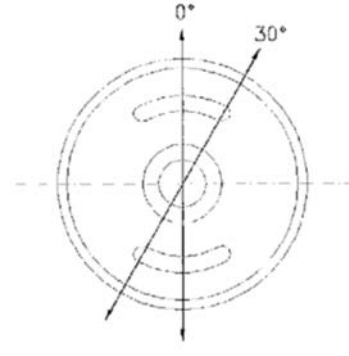

Fig. 18 Loading directions along which the fatigue tests were conducted on a rubber bush

at a size of about 3 mm could be seen by naked eyes.

The hardness of the bush could not be measured by using Durometer type A because the surface of the bush was not flat enough. Instead, the hardness was measured by using micro indenter (ASTM D1415), and it was converted to the hardness that Durometer type A would measure based on the following linear relationship. It has been known that there is a linear relationship between hardness measured by Durometer type A and that measured by the micro indenter (Japanese Chemical Products Examination Committee). Thus, in this study the hardness of heat-aged compression specimens measured by Durometer type A was compared with that measured by the micro indenter, and the following relationship was obtained.

$$D_d = 1.03 D_m - 8.97 \tag{7}$$

Here, D_d is the hardness measued by Durometer type A, and D_m is the hardness measured by the micro indenter.

The fatigue life is shown in Fig. 19 as a function of IRHD. For the loading direction of 0°, the specimens with IRHD below 70 did not fail until 2.6×10^6 cycles, which is double the durability requirement of the bush. However, the fatigue life decreased almost linearly over IRHD of 70. In addition, for the loading direction of 30°, the fatigue life seemed to remain almost the same below IRHD of 70, but it decreased over IRHD of 70. It is noteworthy that the fatigue life is very much dependent on the loading direction, and the trend of the fatigue life of the rubber bush is almost the same as that of the simple shear and the hourglass-shaped specimens.

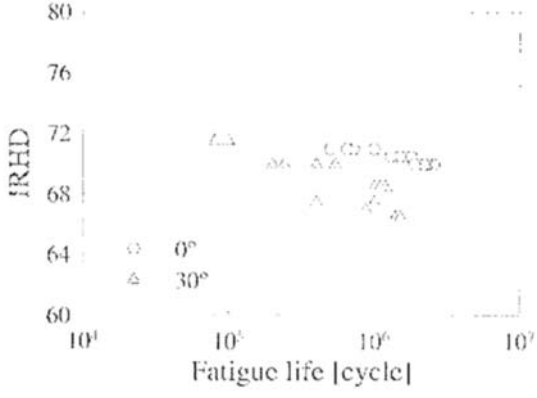

Fig. 19 Fatigue life of a rubber bush for loading directions of 0° and 30°

6. Fatigue Life Prediction Equations

6.1 Fatigue life prediction equations for specimens

If the fatigue life of a rubber component can be predicted based on a physical quantity obtained from an FEM simulation, it will be possible to design the rubber component in a way that the fatigue life is maximized. For metals, the fatigue life has been predicted by using physical quantities such as the effective stress and the effective strain (Collins, 1993). However, for rubbers it has been related to the maximum principal nominal strain (Takeuchi, 1993). In this study, the feasibility of using four physical quantities in the prediction of the fatigue life of rubbers was investigated. The four physical quantities are the effective stress, the strain energy density, the first invariant of the Cauchy-Green deformation tensor and the maximum principal nominal strain. Since the fatigue life seemed to decrease exponentially as the maximum displacement increased (refer to Figs. 13 and 15, and note that the log linear scale is used in the figures), it can be represented as follows.

$$N_f^e = \exp(C_1\xi + C_2) \tag{8}$$

Here, N_f^e is the fatigue life in cycles, ξ is one of the physical quantities, and C_1 and C_2 are constants.

First, the values of the physical quantities occurring in the hourglass-shaped specimen and the simple shear specimen were determined from FE simulations using ABAQUS. The rubber was modeled by using the Mooney Rivlin material model with A_{10} and A_{01} determined in the previous section. The coefficients C_1 and C_2 in Eq. (8) could be determined in a way that Eq. (8) fit the test data of the fatigue life for virgin specimens

shown in Figs. 13 and 15, and the test data of the fatigue life for heat-aged specimens of IRHD below 70 shown in Figs. 16 and 17 (because there is no noticeable difference in the fatigue life between virgin specimens and heat aged specimens of IRHD below 70). Plugging each physical quantity calculated from the FE simulations into Eq. (8) and conducting the least square method, the constants C_1 and C_2 were determined as follows in order for Eq. (8) to have the best fit to the test data.

$$N_f^e = \exp(-0.95\sigma + 15.83) \quad (9)$$

$$N_f^e = \exp(-2.37\omega + 14.55) \quad (10)$$

$$N_f^e = \exp(-3.48I_1 + 24.91) \quad (11)$$

$$N_f^e = \exp(-5.62\varepsilon + 16.20) \quad (12)$$

Here, σ is the effective stress in MPa, ω is the energy density in MJ/m^3, I_1 is the first invariant of the Cauchy-Green deformation tensor, and ε is the maximum principal nominal strain.

Since the fatigue life decreased almost exponentially as IRHD increased over 70 (refer to Figs. 16 and 17), C_2 in Eq. (8) could be assumed as a linear function of IRHD as follows.

$$C_2 = C_{21}\, IRHD + C_{22} \quad (13)$$

Then, the coefficients C_{21} and C_{22} in Eq. (13) could be determined in a way that Eqs. (8) and (13) with C_1 fixed fit the test data of the fatigue life for heat-aged specimens of IRHD over 70 shown in Figs. 16 and 17. Plugging each physical quantity calculated from the FE simulations for the heat-aged specimens into Eq. (8) and conducting the least square method, the constants C_{21} and C_{22} were determined as follows in order for Eqs. (8) and (13) to have the best fit to the test data.

$$N_f^e = \exp(-0.95\sigma - 1.156IRHD + 97.24) \quad (14)$$

$$N_f^e = \exp(-2.37\omega - 1.161IRHD + 95.95) \quad (15)$$

$$N_f^e = \exp(-3.48I_1 - 1.142IRHD + 106.49) \quad (16)$$

$$N_f^e = \exp(-5.62\varepsilon - 1.169IRHD + 97.51) \quad (17)$$

6.2 Comparison of the predicted fatigue life with test data of the bush

An FEM mesh was built as shown in Fig. 20, and ABAQUS/Explicit was used with the rubber modeled by using the Mooney-Rivlin strain potential function. In addition, three dimensional eight node elements were used along with the hourglass control, and the contact between surfaces around the voids was defined by using the surface-surface contact along with the penalty contact algorithm. Note that the Mooney-Rivlin strain potential function was derived from the material properties obtained at the standard tests, but the material properties of natural rubber vary due to different strain rates. Thus, in order to conduct the FE simulation accurately for the bush, the strain rates in the bush must be calculated, and the material properties should be obtained at the strain rates. However, since there are many sets of material properties available for rubber conducted at the standard tests and the strain rate in a rubber component is not uniform, it is easier to conduct an FE simulation for a rubber component using the material properties obtained at the standard tests.

From the FE simulation, the maximum values of the effective stress, the strain energy density, the first invariant of the Cauchy-Green deformation tensor and the maximum principal nominal strain were obtained. The maximum values were plugged into the corresponding fatigue life prediction equations (Eqs. (9) ~ (12) for IRHD ≤ 70 and Eqs. (14) ~ (17) for IRHD ≤ 70), and the

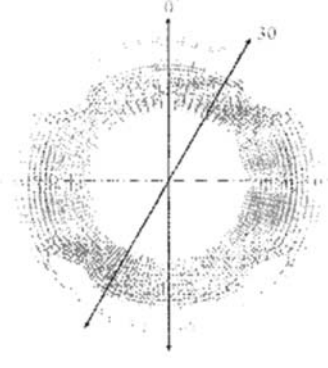

Fig. 20 FEM model for the rubber bush

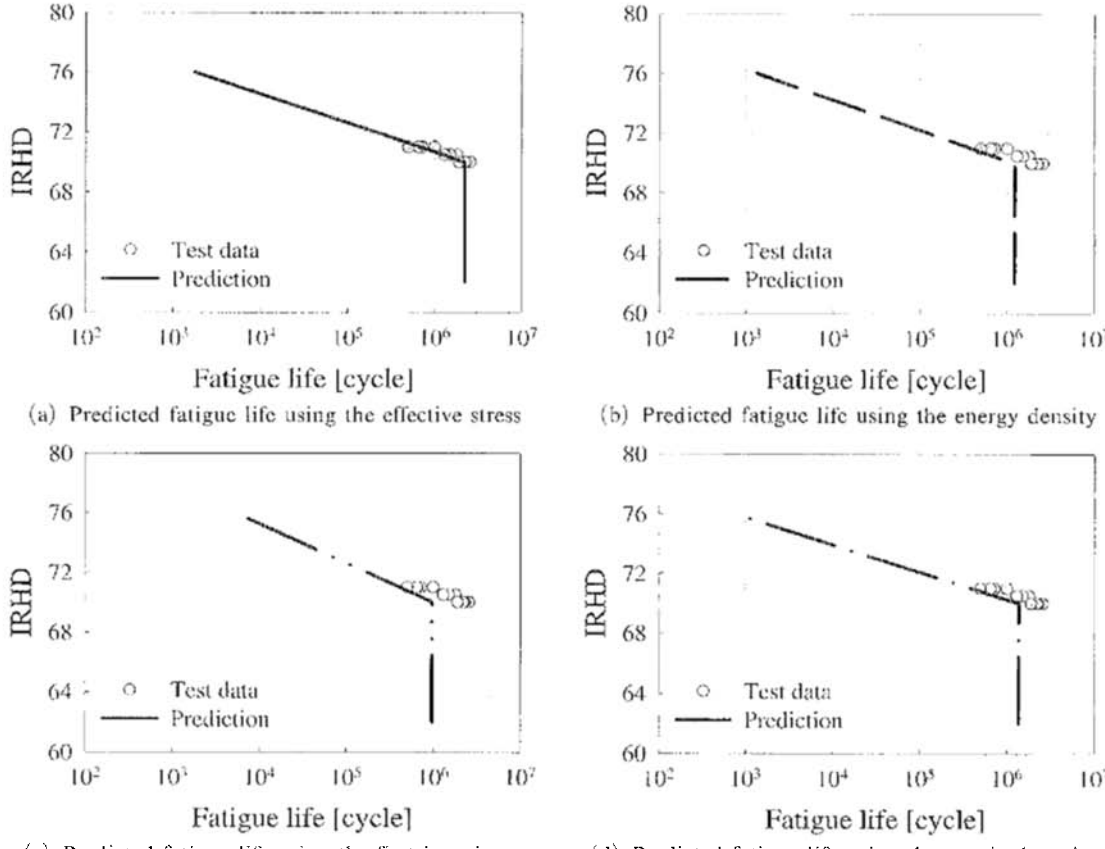

(a) Predicted fatigue life using the effective stress

(b) Predicted fatigue life using the energy density

(c) Predicted fatigue life using the first invariant

(d) Predicted fatigue life using the nominal strain

Fig. 21 Comparison of predicted fatigue life with test data for loading direction of 0°

fatigue life could be predicted. In Fig. 21(a)~(d), the predicted life is plotted by lines, and the test data are shown as symbols for the loading direction of 0°. All of the four prediction equations predicted similar fatigue life for IRHD over 70 although they slightly underestimated the test data. Especially, Eq. (11) using the first invariant predicted the least fatigue life for IRHD below 70. In Fig. 22(a)~(d), the predicted life and the test data are shown for the loading direction of 30°. Eqs. (9) and (14) using the effective stress or Eqs. (10) and (15) using the energy density predicted the fatigue life appropriately both for IRHD below 70 and for IRHD over 70 ; in more detail, Eq. (9) using the effective stress slightly underestimated the fatigue life for IRHD below 70, and Eq. (15) using the energy density slightly overestimated the fatigue life for IRHD over 70. In addition, Eq. (16) using the first invariant or Eq. (17) using the maximum principal nominal strain predicted the fatigue life appropriately for IRHD over 70, but Eq. (11) using the first invariant or Eq. (12) using the maximum principal nominal strain underestimated the fatigue life for IRHD below 70.

Based on the comparison of the predicted fatigue life with the test data for the loading directions of 0° and 30°, it may be said that all the four prediction equations resulted in a similar correlation, but the prediction equation using the effective stress or the energy density resulted in a slightly better correlation. Note that the effective stress is zero under a pure hydrostatic stress. This means that under a cyclic loading of hydrostatic stress a rubber component is predicted to have infinite fatigue life based on the prediction equation using the effective stress, which is not conceptually acceptable. Therefore, the energy densi-

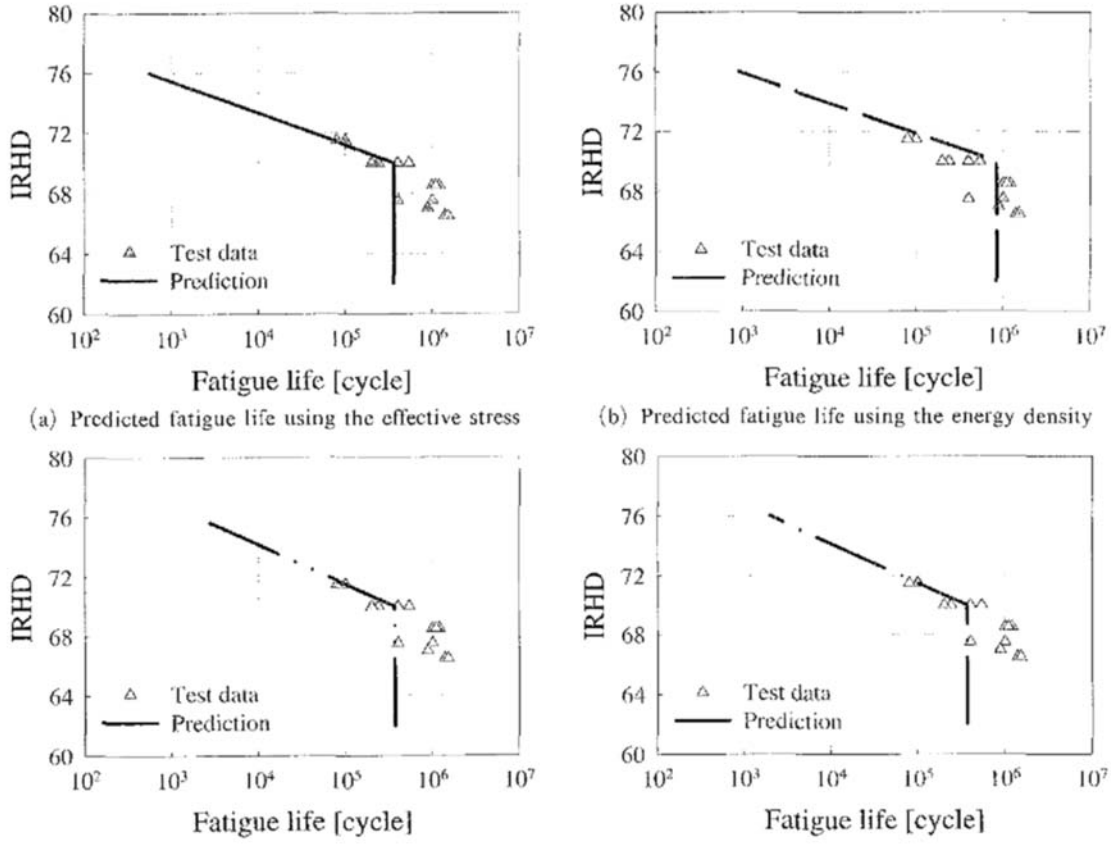

(a) Predicted fatigue life using the effective stress

(b) Predicted fatigue life using the energy density

(c) Predicted fatigue life using the first invariant

(d) Predicted fatigue life using the nominal strain

Fig. 22 Comparison of predicted fatigue life with test data for loading direction of 30°

ty may be considered as the most appropriate controlling physical quantity for the fatigue failure of natural rubber among those four quantities evaluated in this study.

7. Conclusions

Based on the results of this study, several conclusions could be made. First, mechanical conditioning has to be conducted in order to obtain a representative load-stretch ratio curve for natural rubber. Since mechanical conditioning with a different amount of stretch results in a different load-stretch ratio curve, mechanical conditioning has to be conducted with a plausible and fixed amount of stretch. Second, heat-aging usually results in hardening of rubber, and it entails a high load-stretch ratio curve. In contrast, an environment test at a high temperature hardly changes a load-stretch ratio curve. Rather, an environment test at a low temperature results in a high load-stretch ratio curve. Third, the amount of heat-aging was represented by a hardness increase in this study, and the hardness prediction equation proposed in this study resulted in a good correlation with test data for rubber specimens heat-aged subsequently in two different conditions. Finally, four fatigue life prediction equations were proposed by fitting the equations to the test data for hourglass-shaped specimens and simple shear specimens. The predicted fatigue life for a rubber bush used in an automobile from those equations was compared with the corresponding test data. Although all of the four equations resulted in similar fatigue life, the equation using the energy density resulted in the most compatible fatigue life. Therefore, it may be said that the energy density is the most appropriate

controlling physical quantity in the fatigue failure of natural rubber among those four physical quantities evaluated in this study.

Acknowledgments

The specimens were provided by Pyeong Hwa Industrial Company, and this is highly appreciated.

References

ABAQUS, 2001, User's Manual.

ASTM 575-91, "Compression."

ASTM D412-92, 1996, "Standard Test Methods for Vulcanized Rubber and Thermoplastic Rubbers and Thermoplastic Elastomers-Tension," Annual Book of ASTM Standard, pp. 41~53.

ASTM D1415-88, "Rubber-International Hardness."

ASTM D2240-95, "Durometer Hardness."

Brown, R. P., 1986, Physical Testing of Rubber, 2nd ed., pp. 272~275.

Collins, J. A., 1993, Failure of Materials in Mechanical Design, John Wiley & Sons.

Findik, F., Yilmaz, R. and Köksal. T., 2004, "Investigation of Mechanical and Physical Properties of Several Industrial Rubbers," *Materials & Design*, Vol. 25, No. 4, pp. 269~276.

ISO 1827, 1991, Rubber, Vulcanized or Thermoplastic — Determination of Modulus in Shear or Adhesion to Rigid Plates — Quadruple Shear Method.

Japanese Chemical Products Examination Committee, Test Report OA-1620.

Lee, W. B., 1988, Mechanical Component Design, (in Korean).

Miller, M. L., 1966, The Structure of Polymers, Reinhold Publishing Corporation.

Mullins, L., 1969, "Softening of Rubber by Deformation," *Rubber Chemistry and Technology*, Vol. 42, pp. 339~362.

Ogden, R W., 1986, "Recent advances in the phenomenological theory of rubber elasticity," *Rubber Chem. and Tech.*, Vol. 59, pp. 361~383.

Rivlin, R. S., 1956, Rheology — Large Elastic Deformations, Academic Press.

Shen, Y., Golnaraghi, F. and Plumtree, A., 2001, "Modelling Compressive Cyclic Stress-Strain Behavior of Structural Foam," *International Journal of Fatigue*, Vol. 23, pp. 491~497.

Shin, S. J., 1998, Analysis of Rubber-Metal Coupled Problems Using Three-Dimensional Finite Element Methods, Ph. D. Dissertation, Seoul National University.

Takeuchi, K., Nakagawa M., Yamaguchi, H. and Okumoto, T., 1993, "Fatigue Test Technique of Rubber Materials for Vibration Insulators and Their Evaluation," *International Poly. Sci. and Tech.*, Vol. 20, No. 10, pp. T/64-T/69.

Treloar, L. R. G., 1975, The Physics of Rubber Elasticity, Oxford at the Clarendon Press.